TOWARDS THE USE OF ELECTROSPUN PIEZOELECTRIC NANOFIBRE LAYERS FOR ENABLING IN-SITU MEASUREMENT IN HIGH PERFORMANCE COMPOSITE LAMINATES

Saeid Lotfian[1,3], Vijay Thakur Kumar[1], Claire Giraudmaillet[1], Ata Yoosefinejad[2], Feargal Brennan[3], Hamed Yazdani Nezhad[1,*]

[1]Enhanced Composites & Structures Centre, School of Aerospace, Transport and Manufacturing, Cranfield University, MK43 0AL, UK
[2]Munro Technology Limited, Lufton Height Commerce Park, Yeovil, BA22 8UY, UK
[3]Naval Architecture, Ocean & Marine Engineering, University of Strathclyde, G1 1XQ, UK

*Corresponding author: h.yazdani-nezhad@cranfield.ac.uk, Web Page: http://www.cranfield.ac.uk

Keywords: polymer-matrix composite, PVDF, piezoelectric phases, in-situ measurement, structural integrity

Abstract
The aim of this research is to highlight the effects from composite manufacturing on the piezoelectric properties of fibre-reinforced composite laminates internally modified by layers of low-density piezoelectric thermoplastic nanofibres in association with a conductive electrode layer. for in-situ deformation measurement of aerospace and renewable energy composite structures through enabling electrical signal change.

Several methods have been used to analyse the effects such as phase characterisation of the piezoelectric thermoplastic nanofibres and non-destructive inspection of the laminates, during processing an Inter Digital Electrode (IDE) made by conductive epoxy-graphene resin, and pre-preg autoclave manufacturing aerospace grade laminates. The purpose of fabrication of such IDE layer was to embed the same resin type (HexFlow® RTM6) for the conductive layer as that used for the laminates, in order to sustain the structural integrity via mitigation of downgrading effects on the bonding quality and interlaminar properties between plies, rising from materials mismatch and discontinuous interplay stress transfer.

XRD, FTIR, EDS and SEM analyses have been carried out in the material characterisation phase, whereas pulsed thermography and ultrasonic C-scanning were used for the localisation of conductive resin embedded within the composite laminates. This study has shown promising results for enabling internally embedded piezoelectricity (and thus health monitoring capabilities) in high performance composite laminates such as those in aerospace, automotive and energy sectors.

1. Introduction

Various industries such as those in aerospace, automotive and renewable energy sectors intensively use polymer-matrix composite (PMC) materials due to their lightness as well as outstanding mechanical properties. However, safety regulations and reliability assurance of the structural integrity are crucial factors in driving the use of such materials in aircraft and turbine blade structures. To satisfy both, non-destructive inspection (NDI) of the structure is carried out which is complicated and costly inefficient for PMC than that for metallic structures, due to composites' multiple material structure. Moreover, existing NDI techniques are unable to detect zero-thickness interlaminar bond defects (so-called kissing and weak bonds) likely to occur in composite adhesively bonded joints [1-3] or composite laminate manufacturing [4, 5]. Therefore, development of new in-situ measurement and health monitoring techniques is required. Ultrasonic or acoustic piezoelectric sensing have been gathering interest for years, but their low durability, low capability for complex parts and limited strain-to-failure resistivity lessen their possibilities to be considered for long term applications [6, 7]. One promising technique is the fibre optic sensing, which proposes a continuous and real-time health monitoring of composite structures [8], But fibres have relatively low mechanical strength, can irreversibly be damaged or malfunctioned (difficult to repair).

S. Lotfian, V.T. Kumar, C. Giraudmaillet, A. Yoosefinejad, F. Brennan, H. Yazdani Nezhad

In piezoelectric materials, the elastic strain energy of the materials can be related to their dielectric energy. Thus, a proportionality can be established between the mechanical deformation of the materials and a corresponding change in the electrical signals, e.g. change in voltage [9]. Categorised as polymers, they can make ideal candidate to reduce material mismatch in bonding with PMCs (the foundation of the current research) for high performance applications. However due to their particular crystallographic structure, piezoelectric materials are highly anisotropic, which means that the electrical properties vary with the orientation of the crystal [10]. Thus, it is necessary to give orientation to the properties required for directional tailoring. The current paper represents development of a novel technology, applicable to large structures, that uses room temperature, high voltage electrospinning technique to produce ultra-thin unidirectional nanofibres and rapid embedment inside composite laminates.

The nanofibers are made of polyvinylidene fluoride (PVDF) which is a fluoropolymer thermoplastic resulting from the polymerisation of the vinylidene difluoride [10, 11]. PVDF has a semi-crystalline polymorphic structure with five phases: $\alpha, \beta, \gamma, \delta$ and ε. The three first phases are the most commonly used in in-situ measurement applications [12], composed of two types of groups: CF_2 fluorine group (electrically negative) and CH_2 hydrogen group (electrically positive). Depending on the localisation of these groups along the polymer chain, an electrical dipole moment is generated (approx.. 5–8×10^{-30} C.m). Thus, its use is appropriate for sensors development [13].

During the curing process of the laminates, the PVDF material undergoes high temperature ($>T_m$) and constant pressure for a few hours, which entails a new phase transformation. The current paper studies such transformation post process of PMC manufacturing.

2. Materials and Manufacturing

Aerospace grade materials listed in Table 1 were selected for this study.

**Table 1:** Materials used in the study: description and reason of their selection

Material	Commercial	Supplier	Description and properties	Reason of their selection
Unidirectional carbon fibre-reinforced composite	HexPly® M21/35%/268/T700 GC	Hexcel	Aerospace grade, carbon fibre-epoxy pre-preg. Ply thickness: ~0.25mm; Curing temperature: 180°C	High performance laminate, easy to deform, shape and manufacture
PVDF fibres	PVDF FibroTend	Munro Technology Limited	Piezoelectric thermoplastic (PVDF) nanofibres, highly oriented, diameter<1.5μm	Desirable piezoelectric properties of the nanofibres
Epoxy resin	HexFlow® RTM6	Hexcel	Premixed epoxy system. Curing temperature: 180°C	Similar resin to the one composing the pre-preg for good bonding
Graphene powder	CamGraph® G1 A	Cambridge Nanosystems	Ultra-high quality graphene powder. Density: ~26.8g/L	High quality and conductivity; low density

The stacking sequence of the composite laminate was chosen to be symmetric and quasi-isotropic, [-45/+45/90/0]$_S$. Figure 1 schematically shows the main composition of the manufactured laminate. The PVDF layer was set to be embedded just one layer beneath the upper ply of the laminate. That would introduce sufficient justification of internal embedment of an in-situ measurement capability rather than a severe consideration e.g. embedment in the middle layer.

In electrospinning, both melted PVDF material and mixed material powder in a solvent with a gel-like state are used. This raw material chosen is placed in a syringe. The material is progressively pushed in the spinning nozzle tip, where a droplet of material initially forms. Due to a high electrical field applied between the nozzle tip and the collector, the droplet is oriented and stretched up to a nanoscale. This deformation plays on the surface energy of the droplet. The process is continuous, which means that a proper droplet cannot form any longer after the starting phase [14]. According to a study done on

S. Lotfian, V.T. Kumar, C. Giraudmaillet, A. Yoosefinejad, F. Brennan, H. Yazdani Nezhad

stretched PVDF films, the transformation of α phase into β phase seems to be more affected by the stretching ratio than the stretching temperature [15].

Due to the use of aerospace pre-pregnated thermoset composites and autoclave for manufacturing composite laminates, heat energy at high temperature is required for the curing to be effective: approx. 180°C for carbon-fibre pre-pregs and 120°C for glass-fibre pre-pregs. Reticulation occurs between polymer chains which leads to strong bonds within the structure and solidification of the material. The melting temperature of PVDF material is 171°C -175°C, which means that during the carbon-fibre laminate curing, the PVDF fibres will be partially molten. This mean that the piezoelectric capability of PVDF fibres is still valid even after a high temperature exposure. The study in this paper aims to present what piezoelectric capabilities can be left at the post-process stage where the material is solidified for high performance lightweight structural applications.
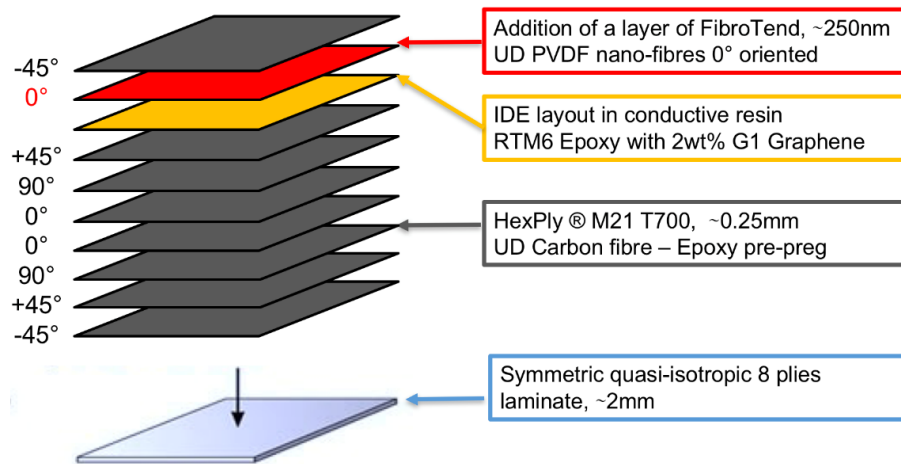

Figure 1: Quasi-isotropic stacking sequence of integrated composite laminates

The IDE layer plays a central role in the laminate for a health-monitoring purpose. The two types of unimorph electrodes (d_{33} and d_{31}) were initially considered. However, due to the porous morphology of the piezoelectric, a reliable electrode with a d_{33} configuration appeared to be too risky: FibroTend layer is ultra-thin ($\sim$250nm-1micron) and composed of numerous fibres, which would easily let a conductive resin flow through it during the curing cycle leading to short circuits. Therefore, the simple d_{33} configuration was abandoned for a d_{31} configuration. The main difficulty was to make sure the IDE would be an integrated part of the laminate to serve structural integrity (i.e. not acting as an external object/defect), by an effective bonding between the IDE and the pre-pregs. This aspect is novel, and such introduction has rarely been exercised. The IDE layout was developed using graphene mixing in a resin (RTM6) similar to that of the composite laminate (M21), over the PVDF layer (Figure 1). Therefore, curing of the resin from both pre-preg and the IDE was done simultaneously to produce strong bonding as the layout was then an integrated part of the structure. However, a drawback in such integration technique was that the layout's resin was allowed to flow during autoclave processing and as such, there was no control on its change of geometry. To avoid possible short circuits during such flow, the authors took a theoretical step for design of the IDE layout with the widest possible spacing according to the recommendations in [16]:

According to the choice of resin dispersion method, the nano-scale dispersion appeared difficult to achieve. Therefore, the electrode layout was scaled up to a millimeter scale, with larger electrode fingers (W_e) and larger finger spacing (S). Also, S should be minimized compared to the width of fingers (W) which should be maximized. The electrode is placed/printed at the center of the length of the sample, and the length of the electrode is limited to fit with the span of the upper clamping fixtures used for applying the mechanical load. This condition is required to ensure that the electrode is not damaged due to the introduction of localised stress from the fixtures in contact with the sample. Therefore, the dimensions of the sample were reviewed for the specific purpose of integrating with the composite laminate, and recommended as below (shown in Figure 2):

S. Lotfian, V.T. Kumar, C. Giraudmaillet, A. Yoosefinejad, F. Brennan, H. Yazdani Nezhad

The width of the sample was increased to 30mm with the electrode width W of 20mm. The electrode finger width W_e was set at 1.5mm, and the spacing between the fingers to 3mm.
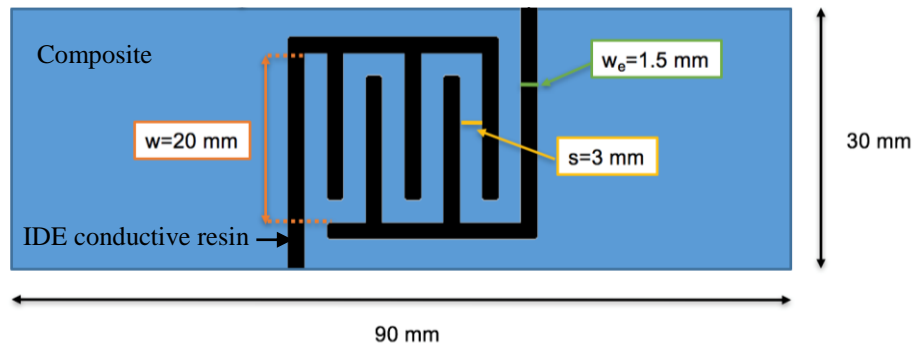

Figure 2: Schematic of the scaled-up IDE electrode layout for composite integration

The graphene was supplied in a powder form supplied by Cambridge Nanosystems (Table 1), for mixing the powder into the epoxy resin. It has been shown that the increasing weight percentage of graphene in resin has an increasing effect on the resin's electrical conductivity, reaching a threshold circa 2wt% graphene filler [17]. Accordingly, the conductivity of the resin examined in this study was increased via high shear mixing of graphene nanopowders, composing of 40g of HexFlow® RTM6 epoxy resin and 0.8g of CamGraph® G1 A graphene powder, which results in an approximately 2wt% concentration. Trials on high shear mixing and ultrasonic exfoliation was carried out to avoid/mitigate the presence of high agglomeration.

The following steps have been followed to manufacture the modified integrated composite laminate:

1) Cutting pre-pregs at the neat size of the final sample (30mm x 90mm), with the relevant orientation of 0°, 45° or 90°.
2) Stacking of the pre-preg pieces in the quasi-isotropic order (Figure 1).
3) Deposition of the conductive resin using jet printing.
4) Finishing the laminate with the last 8th ply on which the piezoelectric FibroTend had already been deposited via electrospinning, as shown in Figure 3.
5) All samples were placed and layed up with the FibroTend layer on top for autoclave processing. In addition of the required release films for vacuum bagging, a metal plate was placed on top of the samples to ensure uniform pressurisation during the curing process.
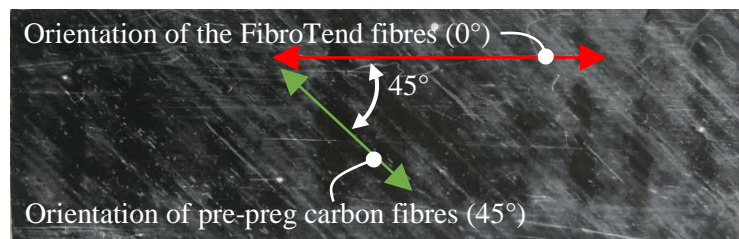
Figure 3: 8th ply, Hexply®M21 carbon composite (45°) with PVDF FibroTend nanofibres on top (0°)

Standard curing cycle according to the Hexply® specifications [18] was conducted. The curing cycle with a heat-up rate of 1°C/min was selected for this study so as to limit the flow of the conductive resin. Viscosity and the resin flow decreases with the duration while temperature constantly increases. The trend in viscosity changes after 100 minutes i.e. it embarks on a sharp increase with time. A low heat-up rate (1°C/min) enables to moderate the viscosity drop until the resin reticulates for times<100 minutes, and thus significantly reduces the chance of flow and short circuits in the integrated laminate. To assess the influence of the laminate modification (i.e. addition of a FibroTend layer and an electrode), eight additional samples were also manufactured with no FibroTend-IDE layer. These samples are referred to as reference samples in this paper.

S. Lotfian, V.T. Kumar, C. Giraudmaillet, A. Yoosefinejad, F. Brennan, H. Yazdani Nezhad

3. Characterisation of PVDF materials

SEM, EDS, XRD and FTIR characterisation techniques were employed for analysis of the morphology and crystal phases of five categories of samples, which are labelled and tabulated in Table 2.

**Table 2:** Five categories of PVDFs used for morphological analysis and phase characterisation

Name	Description
FibroTend 1	Electrospun PVDF fibres stretched +25% and twisted into a bundle
FibroTend 2	Electrospun PVDF fibres stretched to +300% and twisted into a bundle
FibroTend 3	Electrospun PVDF fibres stretched to +300% deposited on aluminum foil, 1.2gsm
PVDF powder	Neat PVDF powder Solvay Solef® 6020/1001
Finetex	Unaligned mat of electrospun PVDF fibres, 8.5gsm

The integrated laminates were also analysed after manufacturing using the characterisation techniques described above. The objectives were to understand the IDE pattern localisation, the FibroTend piezoelectric characteristics after curing, the electrical capability of cured graphene-epoxy resin and the effects of such multi-material integration taken in this study on the mechanical properties. Pulsed thermography, Ultrasonic C-scanning, XRD, FTIR and electrical resistance testing were used for post integration stage of the study.

4. Results and Discussion

4.1. Raw Material characterization

The powders are in homogeneous sphere shape with average diameter of 100μm, as shown in Figure 4a. Finetex sample showed an unaligned mat of fibres (Figure 4b), with average diameters of ~150nm. Some beading and significant variation in the thickness of the fibres can also be observed, as well as no specific trend in orientation. FibroTend 1 bundled fibre sample (stretched by 100mm, 25%) showed different fibre sizes (Figure 4c), with many in excess of 2μm in diameter (average diameter ~2.3μm). FibroTend 2 sample (stretched by 320mm, 300%) clearly showed damaged fibres (Figure 4d) that did not survive the stretching electrospinning process. At present, there is no mechanism for removing these fibres, but as seen in Figure 4d, they pose a relatively minor contamination compared to the bulk of the sample.
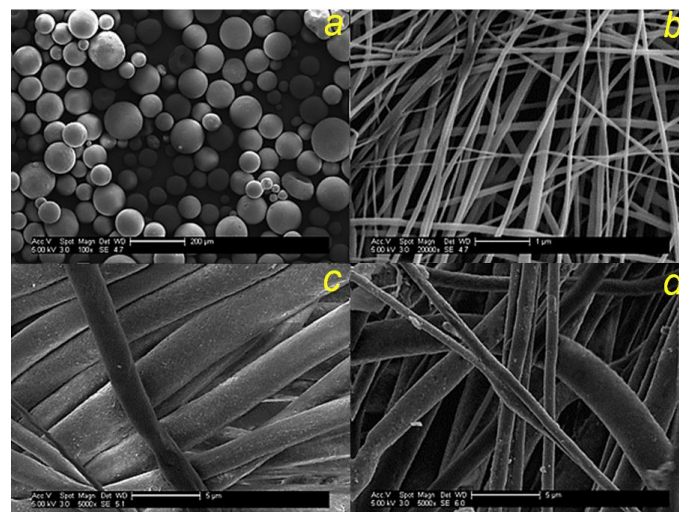
Figure 4: SEM images of (a) PVDF raw powder, (b) Finetex, (c) FibroTend 1, and (d) FiboTend 2

The average fibre diameter was expectedly lower (<1.5μm) for the stretched sample FibroTend 2 than that for FibroTend 1. The FibroTend samples were significantly thicker than the fibres of the Finetex. Also, due to the bundled nature of the samples supplied by Munro Technology Limited, it was not possible to observe the overall trends in fibre alignment.

Energy Dispersive X-ray Spectroscopy (EDS) spectra were collected from the PVDF powder, Finetex and FibroTend 1 & 2. FibroTend 3 was processed precisely identical to FibroTend 2 however on an aluminum substrate, and thus was not characterised. Results from the powder indicated a carbon: fluorine ratio of between 4:1 and 2:1, indicating significant sample contamination, as the expected result was a 1:1 ratio of carbon to fluorine (PVDF unit cell is $-C_2F_2H_2-$). Finetex gave a C:F ratio of 56.5:43.5 based on a relatively large area scan, much closer to the expected values. However, looking at relatively small areas gave much lower values for fluorine content, as low as 15%. That might be explained by a higher detection of the carbon tape on which the Finetex is stuck depending on the sample regions studied (sign of inhomogeneity of the mat porosity). Spectroscopy of the FibroTend fibres (1 and 2) showed a wide range of results across the sample, ranging from 10%-50%, indicating a wide margin of error, perhaps resulting from thin material samples or contamination from handling of the fibres.

The disparity between small-scale and large area measurements indicated that in certain areas of the fibre, carbon-based contamination has occurred to increase the apparent percentage of carbon observed. This contamination can come from manufacturing process, manipulation and detection. As no sample exceeded a fluorine ratio of 50%, it can be assumed that this is an accurate assumption. No peak that could be attributed to any other atomic element than carbon, fluorine or gold (coating) was identified. In particular, no Nitrogen was observed in any of the spectra of the prepared fibres, indicating that a negligible amount of solvent was present.

For determination of the PVDF phases (α, β and γ) present in the material, an X-ray diffraction analysis was carried out [19-22]. The amount of material required to produce a valid data from XRD is hardly compatible with the nano-scale size of the fibres. Therefore, the following procedure was taken:

- Powder: sufficient amount of material and reliable method was used.
- Finetex: a full A4 sheet of PVDF was folded and stuck on a glass holder. Result was acceptable. However, a higher uncertainty of the measurement should be taken into account due to the less dense sample (it is difficult to compress the folded sheet).
- FibroTend 1,2,3: a full A4 amount of PVDF nanofibre was doubled and folded on a glass holder.

Fibres were not grinded into powder due to the risk of the phase change. The spectrums exhibited a similar structure For the three types of PVDF: significant (high intensity) peaks between 17° and 23°, limited (medium intensity) peaks between 24° and 41°, and a flat and non-significant (low intensity) shape elsewhere, as displayed in Figure 5. The measurement were carried out from 10° to 60°, but only a magnified view between 14° and 42° is presented for readability of the report. Note that FibroTend 1 and 2 spectrums are not displayed in the figure as no significant difference can be identified with the FibroTend 3. It implies that the level of electrospinning stretching between +25% and +300% leads to the same crystal composition, thus the same piezoelectricity.
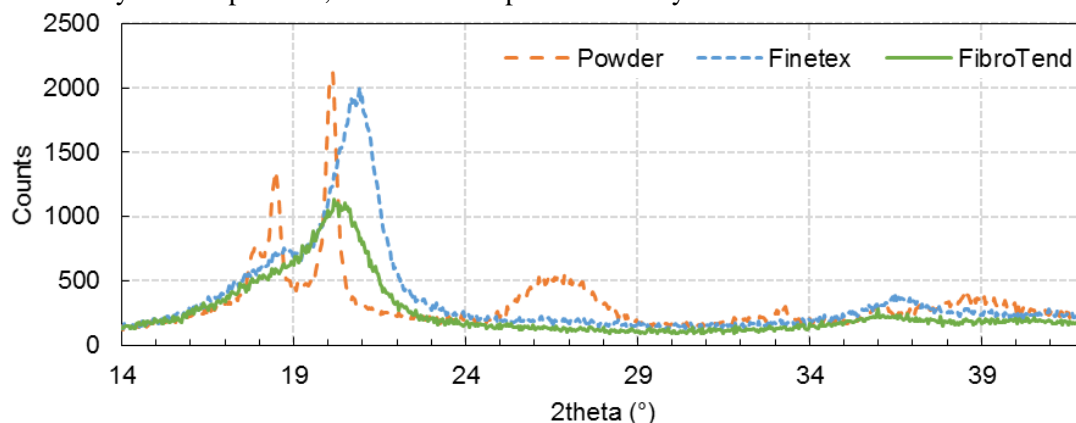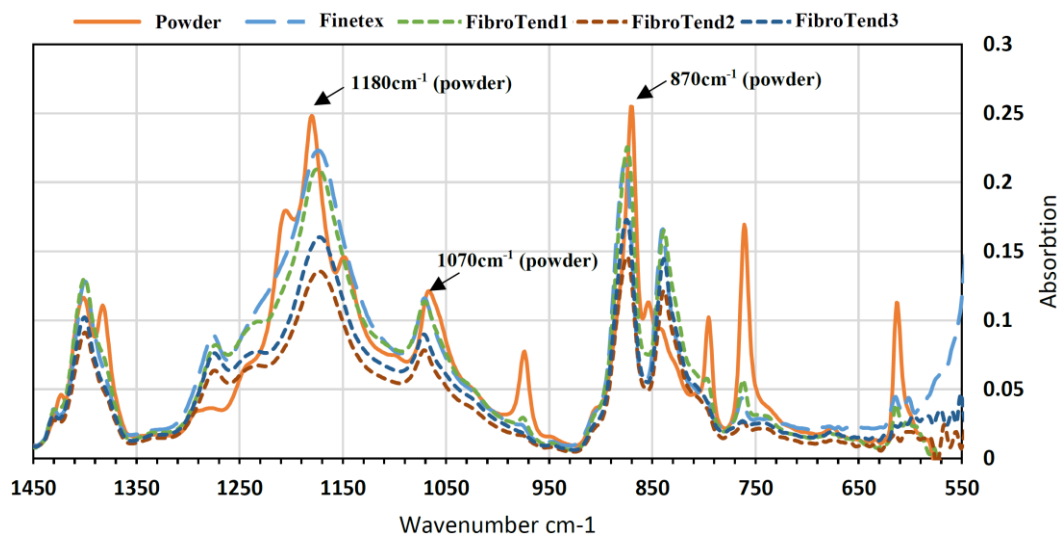

Figure 5: XRD phase spectrums of three forms of analysed PVDF, ranged from 14° to 42°

As seen, some peaks are particularly distinct (high and sharp) whereas others are broader which are difficult to associate them with a single value of angle. In such cases the uncertainty of the spectrum reading and the inaccuracy of the conclusion increase. Table 3 was then extracted collating 2θ angles associated with the peaks observed from each spectrum.

S. Lotfian, V.T. Kumar, C. Giraudmaillet, A. Yoosefinejad, F. Brennan, H. Yazdani Nezhad

Table 3: Summary of XRD phase results for PVDF powder, and electrospun Finetex and FibroTend

Sample	Angle (2θ, °)	Crystal phase associated
Powder	17.9, (20.1), 26.5, 26.8, 36, 39,1	α
	-	β
	18.5, 20.1, 26.8, 38.6	γ
Finetex	-	α
	20.8, 36.5	β
	-	γ
FibroTend	(20.1)	α
	20.3	β
	20.2	γ

The powder spectrum shows that it is mainly composed of α and/or β phases. Some characteristic peaks from those two phases (at 20.1° and 26.8°) are very close to each others which leads to an ambiguous reading of the spectrum. Spectrums are poor for Finetex and FibroTend: only few peaks on each spectrum can be analysed. In addition, these peaks are really broad which does not allow to conclude with a high certainty that both samples, made of the stretched fibres, are composed of β crystal phase. In the Finetex spectrum only β phase characteristic peaks (20.8° and 36.5°) seem to fit with the peaks obtained. Thus, the PVDF sheet is mainly composed of β crystal phase. For FibroTend, the result is less apparent. The single broad peak obtained is associated with the three crystal phases (20.1°, 20.3°, 20.2°). Further characterisation was carried out using FTIR technique that allows to remove the doubt on powder's (α and/or γ) and FibroTend's (β and/or α) phase composition, and confirm the Finetex' β phase composition. It also helps to understand better the proportion of each phase within the material. FTIR wavenumbers (cm^{-1}) analysed in some previous studies for PVDF material were initially studied [21-26]. The absorbance band 840 cm^{-1} can be associated to both β and γ phases due to their really close vibrational frequencies. However a shoulder of the 840 cm^{-1} peak at 833 cm^{-1} can be observed for the γ phase only [27]. To distinguish clearly between the β and γ phases, further comparisons should be considered such as peaks at 1275 cm^{-1} (for β) and 1234 cm^{-1} (for γ), which are specific to each phase. The five experimental spectrums obtained present similar overall spectrums. Figure 6 displays the FTIR ATR ZnSe spectrums of the five forms of the PVDF. Most of the peaks are between 550cm^{-1} and 1450cm^{-1}. Below 550cm^{-1}, the quality of the measurement is dependent on the device.

Figure 6: FTIR spectrums of five forms of PVDF analysed, ranged from 550cm^{-1} to 1450 cm^{-1}

S. Lotfian, V.T. Kumar, C. Giraudmaillet, A. Yoosefinejad, F. Brennan, H. Yazdani Nezhad

Above 1450cm^{-1}, all spectrums are flat with limited peaks. It can be observed that the trend in the appearance of the peaks is the same as for the five spectrums. However, the powder spectrum seems slightly different to the other four, with some peak shifts (around 870, 1070 or 1180 cm^{-1}) and higher additional peaks at approx. 612, 760, 795, 1207 or 1384 cm^{-1}. The powder is the raw material and has not been stretched unlike the other samples. To understand better the impact of electrospinning on the PVDF phase, it is required to compare the powder composition (initial raw material) with the highly stretched processed fibres (e.g. FibroTend 3). Previously the XRD results in Figure 5 and Table 3 showed that the level of electrospinning stretching between +25% (FibroTend 1) and +300% (FibroTend 2, 3) leads to the same crystal composition. This has also been stressed herein by the FTIR data. Table 4 tabulates each spectrum wavenumbers in associated with the peaks observed.

Table 4: Summary of FTIR results for PVDF powder, Finetex and FibroTend 3

Sample	Wavenumber (cm^{-1})	PVDF Phase associated
PVDF Powder	613, 760, 855, 975, 1207, 1383	α
	(846), (1275)	β
	(846)	γ
Finetex	(976), (618)	α
	840, 1175, 1275	β
	840, 1175	γ
FibroTend 3	-	α
	(747), 838, 1168, 1273	β
	(815), 840, 1175, (1236)	γ

To conclude, the PVDF powder is mainly composed of the α phase, with some potential traces of β and γ phases. This is in agreement with the XRD results, so the powder crystal composition can be considered as confirmed and reliable. The Finetex spectrum displays two peaks (840cm^{-1} and 1175cm^{-1}) which are common for the β and γ phases. However, there is a distinct peak at 1275cm^{-1} and no peak at 1234cm^{-1}, which are corresponding to the singular peaks distinguishing β phase from γ phase. This leads to the conclusion, in agreement with the XRD results, which the Finetex sample is mainly composed of β crystal phase. Regarding the FibroTend, many peaks corresponds to β or γ phases. However, β peaks are more dominant (higher than the other representative peaks and more distinct). Therefore, it can be considered that the FibroTend fibres are mainly composed of β phase, though slight γ phase is remaining. This result from XRD and FTIR are logical with the manufacturing process that the PVDF powder, Finetex and FibroTend undergo.

FibroTend was stretched to an average fibre diameter of ~1.5μm whereas Finetex was strechted to <200nm. The α phase is the easiest to produce and the most chemically stable and inert phase, which is a strong interest for commercialisation purpose of raw PVDF powder. The β phase can be achieved after mechanical stretching (herein electrospinning). This process stretches and aligns polymer fibres (Finetex and FibroTend), and leads to a reorganization of the polymer chain.. The γ phase remains from the dissolution of the raw PVDF powder into DMF, preliminary of the electrospinning. The efficiency of the process is not 100%, which justifies why not all the material is made of β phase, and explains the lower traces of γ phase remaining in Finetex.

4.2. Post-processed Material Characterisation

Once composite pre-pregs, PVDF and the conductive IDE layer were layed up, the laminate was cured to integrate the layers. A new set of XRD and FTIR analysis was then carried out to understand the impact of the curing parameters (temperature, duration and pressure) on the PVDF crystal phase, and to

S. Lotfian, V.T. Kumar, C. Giraudmaillet, A. Yoosefinejad, F. Brennan, H. Yazdani Nezhad

identify any piezoelectric remnant phases as curing-linked modification of the phases may lead to reduction of piezoelectricity capability.

However, according to the XRD data, the FibroTend layer embedded between composite plies (~200micron thickness) was too thin (~250nm), and the amount of material was not sufficient for determining the crystal phase. As seen in Figure 7, no peak previously observed with the raw PVDF material (Figure 5) was detected post integration process. Figure 7 shows that the integrated and the reference (with no PVDF-IDE layers) samples have similar spectrums. This confirms that mainly the main laminate structure (carbon fibre and epoxy resin) contributes to the detections. A slight increase (~3%) of the main peak (around 25.5°) was observed for the integrated sample. This is attributed to the detection of the graphene present in the conductive resin forming the conductive layer [28, 29].
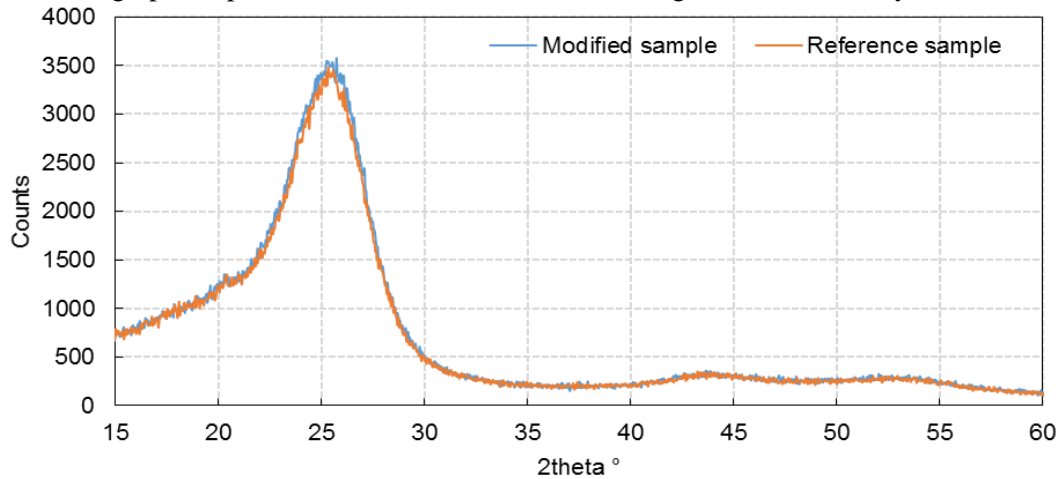
Figure 7: XRD spectrums of both modified and reference composite laminate post integration

FTIR was performed on the integrated and reference samples. Similar to XRD results, no characteristic peak previously seen with the PVDF raw material (Figure 6) can be observed on the integrated sample spectrum, displayed in Figure 8. Also, no significant difference can be observed between the integrated and reference sample spectrums, except a lower intensity of the integrated sample spectrum. This attributes to the presence of additional conductive resin mixed by graphene that absorbs the energy provided for the analysis which lessen the output detected energy.
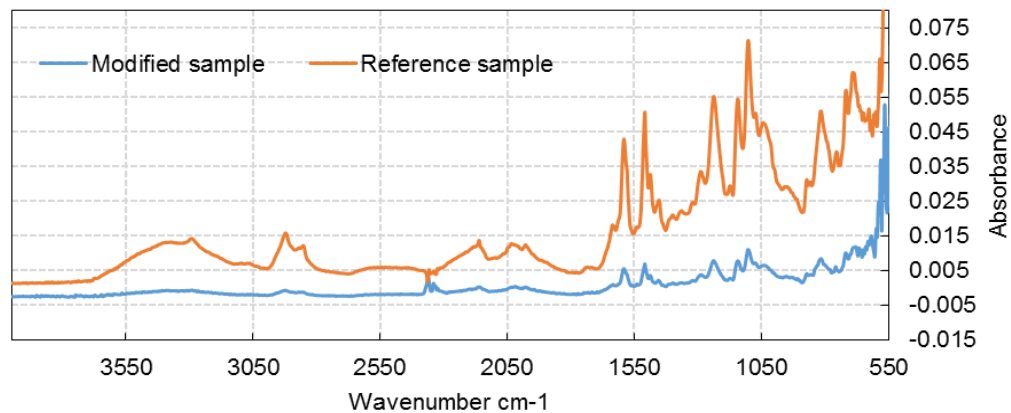
Figure 8: FTIR spectrums of both modified and reference composite laminate

To conclude, post manufacturing material characterisation with XRD and FTIR techniques did not allow to identify the PVDF FibroTend's crystal phase. A new set of experimentations will be highly valuable to understand better the impact of the curing features on the PVDF piezoelectric crystal phase, and also samples with thicker FibroTend layer may provide a clearer spectrum.

S. Lotfian, V.T. Kumar, C. Giraudmaillet, A. Yoosefinejad, F. Brennan, H. Yazdani Nezhad

## 5. Non-destructive inspection data

The NDI data is presented in this section only for the composite laminates integration only, i.e. the two types of integrated laminate (internally embedded with PVDF-conductive layers) and the reference laminate (only composite pre-pregs).

5.1. Pulsed thermography

Two types of comparisons were achieved with the two samples:

1. On the integrated sample, comparison of a region with the central conductive resin and a region without it (at samples runways/corners),
2. Comparison between samples with and without FibroTend-conductive layers.

The pulsed thermography examinations showed that the thermal diffusivity behaviour is different in regions containing or not containing conductive resin, within a sample containing the FibroTend layer (Figure 9). This is due to a difference in thermal conductivity of the two samples linked to the presence of graphene nanomaterials, which in this case is enhanced by the conductive resin (Figure 10). This analysis is to highlight that flash thermography may be interesting to assess the quality of the manufacturing (e.g. curing state) based on the NDI response of the conductive rein.
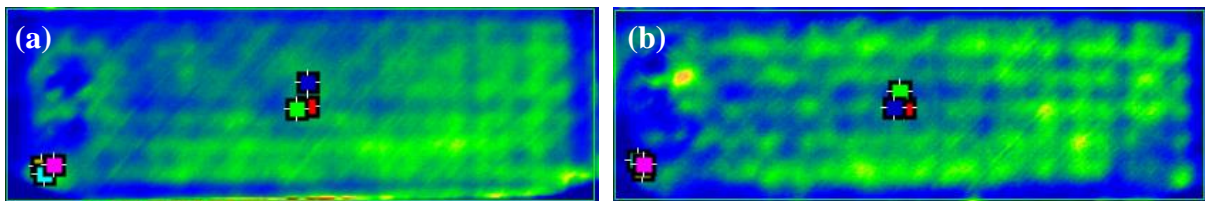

Figure 9: Thermal decay contours at 2 seconds post flashing of the samples; (a) reference sample, (b) integrated laminate sample (with FibroTend-conductive layer) (dimensions of the sample: 30x90mm)
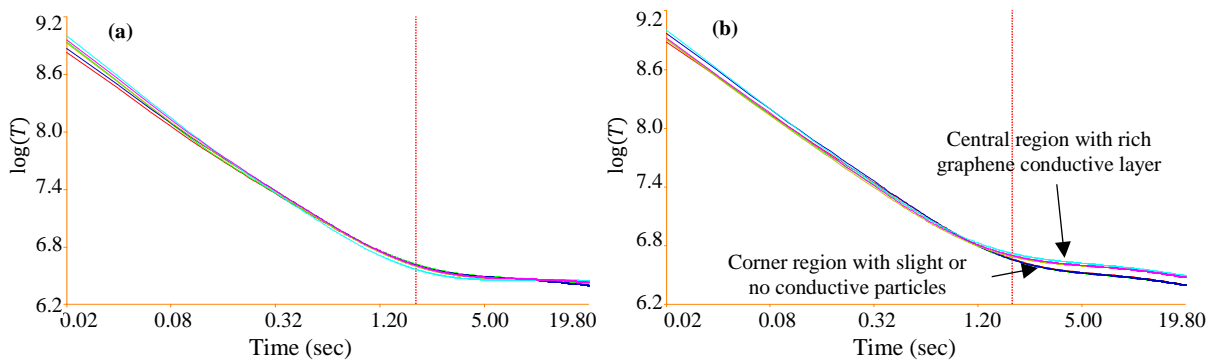

Figure 10: Evolution of thermal decay with time at centre and corner of the samples for (a) reference sample, (b) integrated laminate sample (with FibroTend-conductive layer)

5.2. Ultrasonic C-scanning

Figure 11 and Figure 12 show ultrasound C-scanning images of the reference and integrated samples, respectively. Results for all samples per each type were consistent. Therefore, one representative sample per each type is only shown.
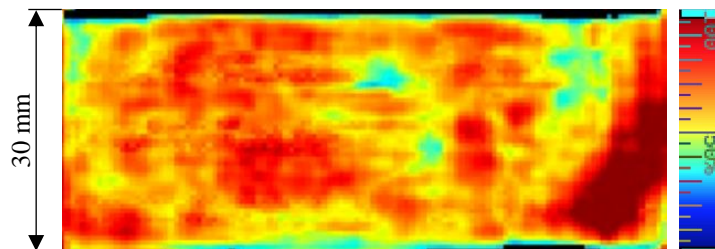
Figure 11: Image of transmission contrast of reference sample

S. Lotfian, V.T. Kumar, C. Giraudmaillet, A. Yoosefinejad, F. Brennan, H. Yazdani Nezhad
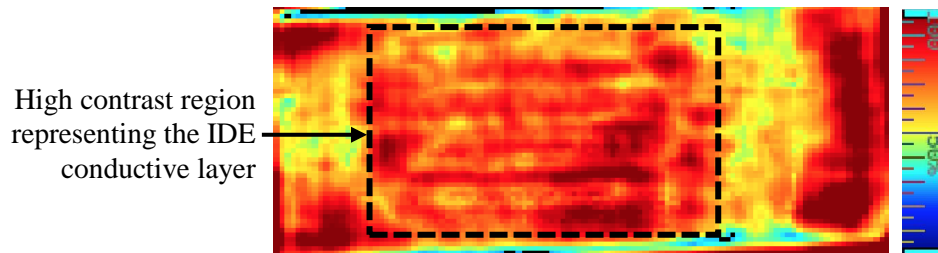
Figure 12: Image of transmission contrast of integrated sample (width of samples: 30mm)

The contrast in Figure 11 is not as high as that in Figure 12 where the conductive layer is present in the integrated laminate. The right edge in both samples and two left corners in the integrated laminate show high contrast which attributes to the carbon composite pre-preg having been bent and damaged during manufacturing. Transmission in Figure 11 is within a 40%-85% range whereas in Figure 12 the transmission rises up to 100%, especially in the central region encompassing the conductive layer. According to literature, epoxy resin has a high transmission coefficient (0.955) compared to any other element composing the sample, e.g. carbon and graphene [30]. This comparison highlight a difference in the composition between the two samples i.e. depending on the composition of the laminate, the intensity of the image can vary. To verify visually that the process effect on the conductive layer's geometric features has been minimal, the integration process was carried out for a transparent glass fibre-reinforced composite (Hexply®913G). Such integration verified that the IDE layout's configuration has properly been preserved post process (not shown in the interest of space).

6. Conclusions

Raw material characterisation before composite laminate manufacturing showed reliable and satisfying results. For PVDF powder, Finetex and FibroTend.

- XRD and FTIR techniques gave in agreement PVDF crystal phase,
- SEM shown satisfying morphology: homogeneous shape and expected size of fibre diameter,
- EDS highlighted a carbon-based contamination level slightly higher than expected.

Regarding the manufacturing of an aerospace laminate modified with a piezoelectric FibroTend layer and a conductive resin electrode (integration process), the main challenges experienced were:

- Achieving a satisfying conductive resin mixture: homogeneous mixing, graphene safety requirements, appropriate viscosity.
- Depositing the conductive resin on pre-preg to form an IDE layout: draw, thickness, accuracy.
- Curing laminate with slight flow of the conductive resin flow (taking a low heating rate).

Post processing analyses were promising:

- In terms of conductive resin localisation, measured by pulsed thermography and ultrasonic C-scanning. In both, a significant difference in thermal decade or transmittance was observed between a zone of the integrated laminate with and without the conductive resin.
- 2wt% graphene-epoxy resin showed efficiency after curing as an electrical resistance was measured.

However, no clear PVDF phase characterisation has been detected post manufacturing: XRD and FTIR techniques did not give exploitable results, due to a too thin FibroTend layer (~250nm).

This investigation showed promising results in terms of preserving geometric features during composite manufacture and integration useful for development of internal in-situ health monitoring of aerospace composite structures. However, the main concept of introducing a piezoelectric layer of PVDF nanofibres and an electrode within a laminate has been supported by a satisfying proportion of piezoelectric β crystal phase of the PVDF raw material (FibroTend), as well as an electrical efficiency of the graphene-epoxy resin after curing. Further analyses on the crystal phase of FibroTend after curing are crucial so as to determine piezoelectricity capability once it's co-processed with composites.

S. Lotfian, V.T. Kumar, C. Giraudmaillet, A. Yoosefinejad, F. Brennan, H. Yazdani Nezhad

Acknowledgments

References

[1]   A. Baker, A. J. Gunnion, and J. Wang, "On the Certification of Bonded Repairs to Primary Composite Aircraft Components," *The Journal of Adhesion,* vol. 91, no. 1-2, pp. 4-38, 2015/01/02 2015.

[2]   R. Bhanushali, D. Ayre, and H. Y. Nezhad, "Tensile Response of Adhesively Bonded Composite-to-composite Single-lap Joints in the Presence of Bond Deficiency," *Procedia CIRP,* vol. 59, pp. 139-143, 2017.

[3]   H. Yazdani Nezhad, Y. Zhao, P. D. Liddel, V. Marchante, and R. Roy, "A novel process-linked assembly failure model for adhesively bonded composite structures," *CIRP Annals,* vol. 66, no. 1, pp. 29-32, 2017/01/01/ 2017.

[4]   H. Yazdani Nezhad, A. Auffray, C. McCarthy, and R. O'Higgins, "Impact damage response of carbon fibre-reinforced aerospace composite panels," 2015: ICCM.

[5]   H. Y. Nezhad, F. Merwick, R. M. Frizzell, and C. T. McCarthy, "Numerical analysis of low-velocity rigid-body impact response of composite panels," (in English), *International Journal of Crashworthiness,* Article vol. 20, no. 1, pp. 27-43, Jan 2015.

[6]   R. Di Sante, "Fibre optic sensors for structural health monitoring of aircraft composite structures: Recent advances and applications," *Sensors,* vol. 15, no. 8, pp. 18666-18713, 2015.

[7]   P. Frontini, S. Lotfian, M. A. Monclús, and J. M. Molina-Aldareguia, "High Temperature Nanoindentation Response of RTM6 Epoxy Resin at Different Strain Rates," *Experimental Mechanics,* journal article vol. 55, no. 5, pp. 851-862, June 01 2015.

[8]   X. Bao and L. Chen, "Recent Progress in Distributed Fiber Optic Sensors," *Sensors,* vol. 12, pp. 8601-8639, 2012.

[9]   P. Ueberschlag, "PVDF piezoelectric polymer," *Sensor review,* vol. 21, no. 2, pp. 118-126, 2001.

[10]   B. Gusarov, "PVDF piezoelectric polymers : characterization and application to thermal energy harvesting," HAL, Grenoble2015.

[11]   J. Yen and R. Amin-Sanayei, "Polyvinylidene fluoride," *Encyclopedia of Chemical Processing,* vol. 1, pp. 2379-2381, 2006.

[12]   S. Mohamadi, "Preparation and Characterization of PVDF/PMMA/Graphene Polymer Blend Nanocomposites by Using ATR-FTIR Technique," Research Gate, Tehran10.5772/36497, 2012.

[13]   H. Correia and M. Ramos, "Quantum modelling of poly(vinylidene flu- oride)," *Computational Materials Science,* vol. 33, no. 1-3, pp. 224-229, 2005.

[14]   M. Leach, Z.-Q. Feng, S. Tuck, and J. Corey, "Electrospinning Fundamentals: Optimizing Solution and Apparatus Parameters," *Journal of Visualized Experiments,* no. 47, January 2011.

[15]   A. Salimi and A. A. Yousefi, "FTIR studies of b-phase crystal formation in stretched PVDF films," Elsevier, Tehran2003.

[16]   R. R. Knight, C. Mo, and W. W. Clark, "MEMS interdigitated electrode pattern optimization for a unimorph piezoelectric beam," *Journal of Electroceram,* vol. 26, pp. 14-22, 2011.

[17]   E. Tkalya, M. Ghislandi, A. Alekseev, C. Koning, and J. Loos, "Latex-based concept for the preparation of graphene-based polymer nanocomposites," *Journal of Materials Chemistry,* January 27 2010.

[18]   "HexPly® M21 180°C (350°F) curing epoxy matrix - Product datasheet," Hexcel corporation2015.

[19]   M. Kanik, O. Aktas, H. S. Sen, E. Durgun, and M. Bayindir, "Spontaneous high piezoelectricity in poly (vinylidene fluoride) nanoribbons produced by iterative thermal size reduction technique," *ACS nano,* vol. 8, no. 9, pp. 9311-9323, 2014.

[20]   E. Kabir, M. Khatun, L. Nasrin, M. J. Raihan, and M. Rahman, "Pure β-phase formation in polyvinylidene fluoride (PVDF)-carbon nanotube composites," *Journal of Physics D: Applied Physics,* vol. 50, no. 16, p. 163002, 2017.

[21]   P. Martins, A. Lopes, and S. Lanceros-Mendez, "Electroactive phases of poly (vinylidene fluoride): determination, processing and applications," *Progress in polymer science,* vol. 39, no. 4, pp. 683-706, 2014.

[22]   Y. Ahn *et al.*, "Enhanced piezoelectric properties of electrospun poly (vinylidene fluoride)/multiwalled carbon nanotube composites due to high β-phase formation in poly (vinylidene fluoride)," *The Journal of Physical Chemistry C,* vol. 117, no. 22, pp. 11791-11799, 2013.

[23]   Y. Li *et al.*, "Multiple stage crystallization of gamma phase poly (vinylidene fluoride) induced by ion-dipole interaction as revealed by time-resolved FTIR and two-dimensional correlation analysis," *Polymer,* vol. 55, no. 18, pp. 4765-4775, 2014.

[24]   S. Lanceros-Mendez, J. Mano, A. Costa, and V. Schmidt, "FTIR and DSC studies of mechanically deformed β-PVDF films," *Journal of Macromolecular Science, Part B,* vol. 40, no. 3-4, pp. 517-527, 2001.

[25]   A. Salimi and A. Yousefi, "Analysis method: FTIR studies of β-phase crystal formation in stretched PVDF films," *Polymer Testing,* vol. 22, no. 6, pp. 699-704, 2003.

[26]   B. S. Ince-Gunduz *et al.*, "Impact of nanosilicates on poly (vinylidene fluoride) crystal polymorphism: Part 1. Melt-crystallization at high supercooling," *Polymer,* vol. 51, no. 6, pp. 1485-1493, 2010.

[27]   P. Martins, A. C. Lopes, and S. Lanceros-Mendez, "Electroactive phases of poly(vinylidene fluoride): Determination, processing and applications," *Progress in Polymer Science,* vol. 39, pp. 683-706, 2014.

[28]   A. Avila, F., L. Peixoto, G., Z. de O., A. Silva Neto, J. de Avila Junior, and M. Carvalho, G., R, "Bending Investigation on Carbon Fiber/Epoxy Composites Nano- Modified by Graphene," *Journal of the Brazilian Society of Mechanical Sciences & Engineering,* vol. 34, no. 3, pp. 269-275, July-September 2012.

[29]   A. Silva Neto, D. Lopes da Cruz, Thadeu, and A. Avila, Ferreira, "Nano-modified Adhesive by Graphene: The Single Lap-Joint Case," *Materials Research,* vol. 16, no. 3, pp. 592-596, November 2013.

[30]   A. Fahr and A. Y. Kandeil, "Ultrasonic C-scan inspection of composite materials," *Engineering Journal of Qatar University,* vol. 5, pp. 201-222, 1992.

Towards the use of electrospun piezoelectric nanofibre layers for enabling in-situ measurement in high performance composite laminates

Lotfian, Saeid

2018-06-30